ACS APPLIED MATERIALS & INTERFACES

Research Article

www.acsami.org

Copper-Encapsulated Vertically Aligned Carbon Nanotube Arrays

Kelly L. Stano,[†] Rachel Chapla,[†] Murphy Carroll,[†] Joshua Nowak,[‡] Marian McCord,[†,§,∥] and Philip D. Bradford*[,†]

[†]Department of Textile Engineering, Chemistry and Science, North Carolina State University, Raleigh, North Carolina 27695-8301, United States

[‡]Department of Nuclear Engineering, North Carolina State University, Raleigh, North Carolina 27695-7909, United States

[§]Joint Department of Biomedical Engineering, North Carolina State University, Raleigh, North Carolina 27695-7115, United States

[∥]University of North Carolina, Chapel Hill, North Carolina 27599, United States

Supporting Information

ABSTRACT: A new procedure is described for the fabrication of vertically aligned carbon nanotubes (VACNTs) that are decorated, and even completely encapsulated, by a dense network of copper nanoparticles. The process involves the conformal deposition of pyrolytic carbon (Py-C) to stabilize the aligned carbon-nanotube structure during processing. The stabilized arrays are mildly functionalized using oxygen plasma treatment to improve wettability, and they are then infiltrated with an aqueous, supersaturated Cu salt solution. Once dried, the salt forms a stabilizing crystal network throughout the array. After calcination and H_2 reduction, Cu nanoparticles are left decorating the CNT surfaces. Studies were carried out to determine the optimal processing parameters to maximize Cu content in the composite. These included the duration of Py-C deposition and system process pressure as well as the implementation of subsequent and multiple Cu salt solution infiltrations. The optimized procedure yielded a nanoscale hybrid material where the anisotropic alignment from the VACNT array was preserved, and the mass of the stabilized arrays was increased by over 24-fold because of the addition of Cu. The procedure has been adapted for other Cu salts and can also be used for other metal salts altogether, including Ni, Co, Fe, and Ag. The resulting composite is ideally suited for application in thermal management devices because of its low density, mechanical integrity, and potentially high thermal conductivity. Additionally, further processing of the material via pressing and sintering can yield consolidated, dense bulk composites.

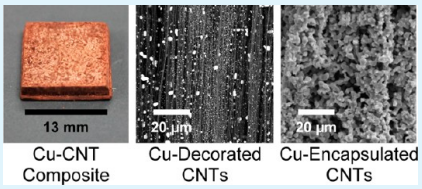

KEYWORDS: *carbon nanotube, nanocomposites, copper, CNT array, thermal management*

1. INTRODUCTION

Hybrid and composite carbon nanotube (CNT)−metal matrix materials are attractive nanostructures for a variety of applications including catalysis agents in fuel cells and batteries,[1−3] electronic sensors,[4−6] hydrogen storage,[7,8] and antimicrobial agents.[9] CNTs are an ideal template on which to fix metal nanoparticles because of their high surface area. In addition to being low density, their stellar mechanical, electrical, and thermal properties have made CNTs a desirable reinforcement in metal matrix composites (MMCs) as well. Metals and their alloys have dominated the structural landscape for decades, but increasing energy demands and declining oil supplies have motivated researchers to develop lighter structural materials with multifunctional capabilities. More specifically, CNT−copper composite hybrid materials, with low coefficients of thermal expansion and high thermal conductivity, are particularly attractive for electronics packaging and thermal management applications.[10−13]

Successful fabrication of these composites has not been straightforward, however, because of highly incompatible processing temperatures and pressures between Cu and CNTs. The extreme conditions required for many traditional metallurgical techniques lead to physical and chemical degradation of the CNT structure and a subsequent worsening of properties in the resulting composite material. Current techniques for fabricating these types of hybrid structures include powder metallurgy,[14−18] electrochemical methods,[19−22] direct thermal decomposition of Cu salts[23] and oxides,[24] and H_2 reduction of surface-adsorbed Cu salt.[25−28] Nearly all studies on Cu-CNT hybrid materials and composites involve the use of short, randomly aligned CNTs in the form of a powder, which are then mixed with Cu powders or precursor. There are many processing difficulties that accompany the use of CNTs in this form, namely, the inability to adequately separate and mix the CNTs homogeneously throughout the Cu matrix. CNTs, with their ultrahigh surface area and therefore large van der Waals attractions, will agglomerate and bundle with their near neighbors. Once bundled, it is very difficult to achieve a stable dispersion or homogeneous mixture without using aggressive treatments like chemical functionalization or ultrasonication. These measures are known to be damaging to the wall structure and degrading to the desirable electrical,

Received: July 22, 2013
Accepted: October 4, 2013
Published: October 4, 2013

mechanical, and thermal properties of pristine CNTs. Because of the anisotropic nature of CNTs' physical properties along their axis, it is often desirable to have preferential alignment of the CNTs in the matrix, although processing routes that can successfully do so are scarce.

In this light, the utilization of vertically aligned CNT arrays (VACNTs) is an attractive alternative to bundled and agglomerated CNT powders. Using catalytic chemical vapor deposition (CVD), VACNTs can be quickly and easily grown with lengths in excess of several millimeters while also being dispersed and minimally bundled. A review of the literature provided only one other study where VACNT arrays were used as Cu matrix reinforcement. Chai et al. used electrodeposition to "fill" an array patterned with vias to allow for easier filling.[29] This method is procedurally complicated, however, requiring complex yet precise bath chemistries. Additionally, because of increased current density at the outside of the array, preferential deposition occurs at the exterior surfaces, creating a Cu cap rather than filling the high aspect ratio voids between CNTs. Though the array height was not mentioned in this most recent work, earlier publications demonstrated difficulty in filling a carbon nanofiber array that measured only 7.5 μm tall.[12] Electrodeposition is neither suitable for applications where the aspect ratio of the CNTs is large nor for bulk preparation of composite material.

It is apparent that alternate processing techniques must be investigated to realize the extraordinary potential of CNT-Cu hybrid structures. This study details a novel procedure for the fabrication of 2 mm tall VACNTs, which are heavily decorated or even encapsulated by a Cu nanoparticle matrix. In this process, VACNT arrays are deposited with pyrolytic carbon (Py-C) to improve their mechanical resilience and dimensional stability. The stabilized arrays are made hydrophilic via oxygen plasma functionalization before being infiltrated with super-saturated Cu salt solution. The samples are dried, leaving behind a network of Cu salt crystals dispersed throughout the VACNT array. The composites are then calcinated and reduced in H_2 to convert the Cu^{2+} ions to Cu metal nanoparticles. Repeating the process cycle further increases Cu content within the VACNT array and causes the nanoparticles to grow and merge. This forms an interconnected shell of Cu that completely encapsulates individual CNTs and CNT bundles while still retaining the vertically aligned array structure. This sample morphology is particularly unique and useful because of the CNT alignment. In developing this new procedure, various factors were examined with the goal of maximizing the final Cu fraction in the composite. These included the duration of Py-C deposition, Cu salt type, calcination and reduction pressures, and implementation of subsequent infiltrations.

2. EXPERIMENTAL SECTION

2.1. Materials. Two millimeter tall VACNT arrays were grown in-house and further processed in preparation for composite fabrication (see procedure below). Copper(II) nitrate (99%+), copper(II) chloride dihydrate (99%+), and copper(II) sulfate pentahydrate (99%+) were purchased from VWR and used without any further purification.

2.2. Measurements. Scanning electron microscopy (SEM) was conducted on a FEI Phenom microscope and a Hitachi S3200 variable pressure scanning electron microscope (VPSEM) fitted with a 4Pi Isis energy-dispersive spectrometer (EDS) system. Elemental spectra were gathered over an acquisition time of 100 s, and accompanying images were taken with a beam voltage of 20 kV. Transmission electron microscopy (TEM) images were taken using a Hitachi HF2000 cold field-emission TEM with a beam voltage of 200 kV. A probe sonicator was used to disperse 0.001 g of CNTs in 10 mL of DI water. To achieve a more stable dispersion, 0.04 g of Triton X-100 surfactant was added. The mixture was pulse-sonicated (1 s on, 0.3 s off) in an ice bath for 1 h. Immediately following sonication, a small amount of the dispersion was deposited on holey carbon mesh Cu TEM grids and then allowed to dry. The graphitic quality and defect density of the CNT arrays was analyzed using a Renishaw Ramascope with a laser wavelength of 514 nm. The laser spot was focused using a Renishaw microscope. X-ray diffraction (XRD) measurements were conducted on a Rigaku SmartLab Bragg−Brentano XRD with a Cu Kα radiation source (λ = 1.5418 Å). Step scans were performed for 2θ = 10−80° with a step width of 0.1° and a scan speed of 4 s. To measure the static contact angle of pristine and post-treated arrays, a Dataphysics OCA 20 contact angle system was used. Live video taken during the measurement allowed for precise calculation of the contact angle by optical measuring software. The volume for all droplets used was 4 μL, which was dispensed at a rate of 1 μL/second.

2.3. Methods. *2.3.1. VACNT Array Preparation.* VACNT arrays were grown on quartz substrates via chlorine-mediated low-pressure chemical vapor deposition (CVD) using iron(II) chloride, anhydrous (99.5%, VWR) catalyst and acetylene carbon precursor.[30] After 20 min of growth, the resulting arrays were ∼2 mm tall with an average MWCNT diameter ∼43 nm, as measured from TEM images. After growth, the VACNT arrays underwent post-treatment to prepare them for the composite fabrication procedure. First, the VACNTs were conformally coated with Py-C using CVD. Samples were heated under vacuum in a quartz tube furnace. At 800 °C, C_2H_2 began to flow at 600 sccm, and the pressure of the system was maintained at 30 Torr. After the desired deposition time (0, 5, 30, or 60 min), the C_2H_2 flow was stopped, and the system was cooled while being purged with Ar gas. These samples are labeled and referred to as Py-C_0, Py-C_5, Py-C_30, and Py-C_60, respectively. Second, the stabilized VACNT arrays were treated with O_2 plasma in a capacitively coupled dielectric barrier discharge atmospheric pressure plasma system. The system consists of two parallel Cu plate electrodes (60 × 60 cm) with a constant spacing of 3 cm. The plasma was operated by a 4.8 kW audio frequency power supply at 1.67 kHz. All treatments were carried out for 30 s in a 1% oxygen + 99% helium gas mixture (by mass).

2.3.2. Cu-VACNT Composite Fabrication. Supersaturated copper-(II) nitrate-salt solution was prepared in a glass jar by stirring the salt and DI water on a magnetic hot plate set to 225 °C. Additional salt was added until the upper solubility limit was reached. The post-treated arrays were infiltrated with solution for 10 s and then dried isothermally at 105 °C in a vacuum oven (MTI Corporation DFA-2000 vacuum oven) for 12 h. Calcination and H_2 reduction experiments were carried out at both atmospheric and reduced pressures to compare the resulting Cu content in the VACNT arrays. For processing at reduced pressure (Cu-VACNT_Vac), the Cu-salt-VACNT composites were dehydrated and calcinated under vacuum at 185 °C for 30 min. To complete the reduction, the sample was then heated at 300 °C while H_2 was flowed at 500 sccm for 30 min and the reaction chamber was regulated to be 95 Torr. In the atmospheric pressure procedure (Cu-VACNT_Atm), calcination was carried out under a 1000 sccm flow of Ar at 225 °C while reduction was completed at 450 °C in a mixture of 1000 sccm Ar and 100 sccm H_2. Calcination and reduction temperatures were selected on the basis of experimental results from the literature.[31−37] Conversion of $Cu(NO_3)_2$ to CuO and Cu occurs at lower temperatures when processing at reduced pressure. The minimum temperature where successful conversion could occur for each pressure was selected to minimize sublimation of the salt from the VACNT arrays.

One major goal of this work was to maximize the Cu content in the VACNT arrays. This was accomplished by introducing a reinfiltration step to the composite fabrication procedure. Experiments were carried out to determine the optimal processing step for this to occur. These included reinfiltration after drying (2Cu-VACNT_Dry), calcination (2Cu-VACNT_Cal), and reduction (2Cu-VACNT_Red). Following reinfiltration, the composites were calcinated and reduced following the procedure outlined above.

3. RESULTS AND DISCUSSION

3.1. Post-treatments for VACNT Array Optimization. Prior to composite fabrication, pristine VACNT arrays were post-treated to optimize their physical and chemical structure for the proposed technique. First, Py-C was deposited on to the VACNT arrays via CVD. Arrays were treated for 0, 5, 30, and 60 min, which yielded linear increases in both array mass and density. Figure 1 shows the CNT array before and after 30 min of Py-C deposition where the average CNT diameter increased from 44 to 63 nm with standard deviations of 9 and 7 nm, respectively. After only 5 min of deposition, the arrays exhibited foamlike recovery after compression, with full recovery exhibited after 30 min of treatment. Observation under TEM showed the Py-C deposited onto the CNTs wall with a laminar-type morphology, creating additional concentric walls with a good degree of graphitization.

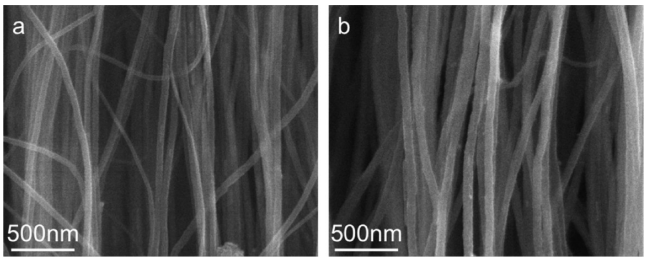

Figure 1. SEM images show as-grown VACNTs (A) with an average diameter of 43.5 nm. After 30 min of Py-C deposition (B), the average diameter of the VACNTs increased to 63.4 nm.

Py-C deposition on VACNTs has been shown to increase the compressive strength of VACNT arrays, even providing strain recovery and foamlike properties as discussed by Bradford et al.[38] In short, Py-C-coated CNTs experience radial diameter growth because of the assembly of additional graphitic walls on the CNT surface, simultaneously increasing surface roughness. Added roughness reduces mutual van der Waals attractions between adjacent CNTs, whereas a larger diameter increases the CNTs' resistance to buckling under compressive load, thus increasing the compressive strength. By optimizing the deposition parameters, it is possible to tune the compressive properties of the array such that the CNT resistance to buckling overcomes the van der Waals attractions and arrays demonstrate foamlike recovery behavior. This study will further demonstrate that Py-C deposition on VACNT arrays has a stabilizing effect when the arrays are subjected to liquid-based processing such as solution infiltration and drying. This is the first example in the literature of Py-C stabilization being utilized for this purpose.

A significant issue to overcome was the physical and chemical hydrophobic nature of the CNT arrays.[39−41] CNTs grown via CVD are known to be chemically inert because of the presence of nonpolar C−H terminations on their surfaces.[42−44] Additionally, VACNT arrays, with their hierarchical micro- and nanosized features, exhibit what is known as the Lotus leaf effect where surface chemistry and morphology combine to create a superhydrophobic, self-cleaning material.[45] Many methods have been developed to promote wetting of CNTs by attaching oxygen-rich functional groups to their surfaces.[46] This is accomplished by oxidizing the CNTs using strong acid, electrical current, or thermal energy. The functionalized CNTs are indeed hydrophilic, but this is accompanied by the introduction of defects to the CNT structure and subsequent decrease in the mechanical, electrical, and thermal properties when compared to pristine CNTs. Furthermore, overcoming this hydrophobicity has an added layer of complexity if the delicate, aligned structure of the VACNT array is to be preserved. Liquid-based chemical oxidation creates significant capillary forces in between adjacent CNTs within the array. Upon drying, the liquid surface tension will drastically disrupt alignment and induce CNT bundling (both of which are undesirable for composite fabrication).

These issues were addressed by using atmospheric pressure oxygen plasma treatments to mildly functionalize the CNTs. In only 1 s of the treatment, the static contact angle (SCA) of a CNT array decreased from an average initial value of 138.2° to 128.1°, and 5 s of plasma exposure was adequate to create a fully wettable array (SCA = 0°). Raman analysis was used to probe the extent of defects incurred as a result of the plasma treatment. Of primary interest are the carbon material disorder induced D-band (1350 cm^{-1})[47] and the G-band (1582 cm^{-1}), which arises from in-plane vibrations of graphite.[48] It is common to compare the ratio of the intensities of these peaks (G_I/D_I) among samples to determine relative defect content and even the extent of chemical functionalization.[49] Generally, a lower value for the G_I/D_I ratio relates to greater defect density or disorder. High surface energy defects act as reactive sites where it is possible to covalently attach functional groups to alter the pristine CNT surface chemistry. Broadening of the D-band relates to the functionalization of CNT sidewalls or tips because of the conversion of sp^2-hybridized C−C bonds to sp^3-hybridized C−X bonds where X may be a functional carbonyl or carboxyl group or simply an H termination to form amorphous carbon.[50] Increased defects will also degrade the mechanical, thermal, and electrical properties of the CNTs, however. Thus, the extent of this damage should be minimized for matrix property enhancement in composite applications.

The average G_I/D_I ratio for pristine arrays was 1.48, whereas that for plasma treated arrays was 1.32. The minimal change in the G_I/D_I ratio was smaller compared to that measured from treatment with other functionalization techniques in the literature.[51] Py-C stabilized arrays coated for 30 min had a lower initial G_I/D_I ratio (0.93) because of the presence of sp^3 carbon on the CNT surface. After plasma treatment, the average G_I/D_I ratio was 0.96. Previous research in plasma functionalization of VACNT arrays found that the ratio could actually be increased because of the plasma interaction with defect-ridden CNT tips, effectively reducing the defect density.[52] In fact, there are competing reactions because of the simultaneous conversion of sp^2 to sp^3 carbon as a result of functionalization.[47] A virtually unchanging G_I/D_I ratio signifies a constant defect density. VACNT arrays were made fully hydrophilic in a matter of seconds through the attachment of polar, oxygen-containing groups to the CNT surfaces via O_2 plasma treatment. Raman analysis confirmed that this was accomplished with little to no change in defect density. Finally, the gas-phase functionalization technique prevented destruction of CNT alignment within the array.

3.2. Fabrication of Copper Nanoparticle Filled VACNT Arrays. Calcination and reduction procedures were conducted on pure $Cu(NO_3)_2$ salt to confirm successful conversion to CuO and Cu. As shown in Figure S1 (Supporting Information), the EDS spectrum of the as-received salt indicates the presence of Cu, N, and O. After heating the salt at 185 °C under vacuum, only Cu and O were detected. Finally, after reduction in H_2 at

300 °C, only Cu remained, thus confirming the full conversion to metallic Cu powder. The same procedure was applied to the infiltrated VACNT arrays for processing.

Immediately following plasma treatment, Py-C-stabilized VACNT arrays were infiltrated with aqueous Cu salt solution. Not only was the plasma treatment necessary for wetting of the array but also the addition of oxygen-containing functional groups to the CNT surfaces allowed for interaction and potential bonding between the Cu ions and CNTs. Boiling hot, supersaturated Cu salt solutions were used for infiltration as opposed to less concentrated solutions at room temperature. The solubility limit of copper(II) nitrate increases for higher solution temperatures, from 59.2 g/100 mL at 25 °C to 71 g/100 mL at 100 °C. This ensured maximum Cu^{2+} ion content postinfiltration. Additionally, as the supersaturated solution cooled, it crystallized to form a stabilizing, interpenetrating network of salt crystals throughout the VACNT array. The solid, dense network filled the many void spaces between CNTs and prevented agglomeration and bundling upon drying. During initial trials with low concentration solutions, the composite was prone to significant cracking and shrinking during the drying step because of the absence of a dense Cu salt network. As presented in the next paragraph, only when arrays were both Py-C-stabilized and infiltrated with supersaturated Cu salt solution could microscopic CNT alignment and macroscopic array structure and dimensions be preserved.

As shown in Figure 2, the duration of Py-C stabilization proved highly influential in the stability and resulting morphology of the Cu-VACNT composites. Hybrid materials were successfully formed at all levels of CVD stabilization, but macroscopic cracks were formed in VACNT arrays treated for less than 30 min (Py-C_0 and Py-C_5). The superior stability of sample Py-C_30, however, is clearly visible after being infiltrated as well as calcinated and reduced. Figure 3 shows that the uptake and retention of Cu salt solution into CVD stabilized arrays was higher compared to VACNT arrays without any stabilization (Py-C_0). Maximum Cu content was achieved for Py-C_30, yielding a composite with 92 wt % Cu. These results (summarized in Figure 3) were attributed to the mechanical stabilization provided by Py-C deposition. Typically, when VACNT arrays are subjected to liquid-based processes, strong capillary forces are generated between adjacent CNTs, especially during drying. This effect causes bundling and agglomeration of CNTs, leading to densification of the array. The foamlike VACNT arrays that were created for longer Py-C deposition times, combined with the reinforcement from the dense Cu salt crystal network, were able to overcome these forces and maintain a dimensionally stable and dispersed structure throughout all steps of the composite process. It is worth noting that CVD stabilization is indeed not necessary to form a hybrid Cu-VACNT structure unless it is desired to retain the alignment and anisotropy of the pristine array structure. In a scenario where the Cu-VACNT composite will be further processed by pressing or sintering, CVD stabilization is not required.

An identical procedure was applied to fabricate larger composites (up to 1 in. square) and to evaluate composites made with other Cu salts ($CuCl_2$ and $CuSO_4$). This yielded similar results as those shown in Figure S2. $Cu(NO_3)_2$ was selected for the majority of this study because of its significantly higher solubility in water and thus higher Cu concentration in the final composite. Additionally, by simply altering the reduction temperature, H_2 can be used to reduce the salts of

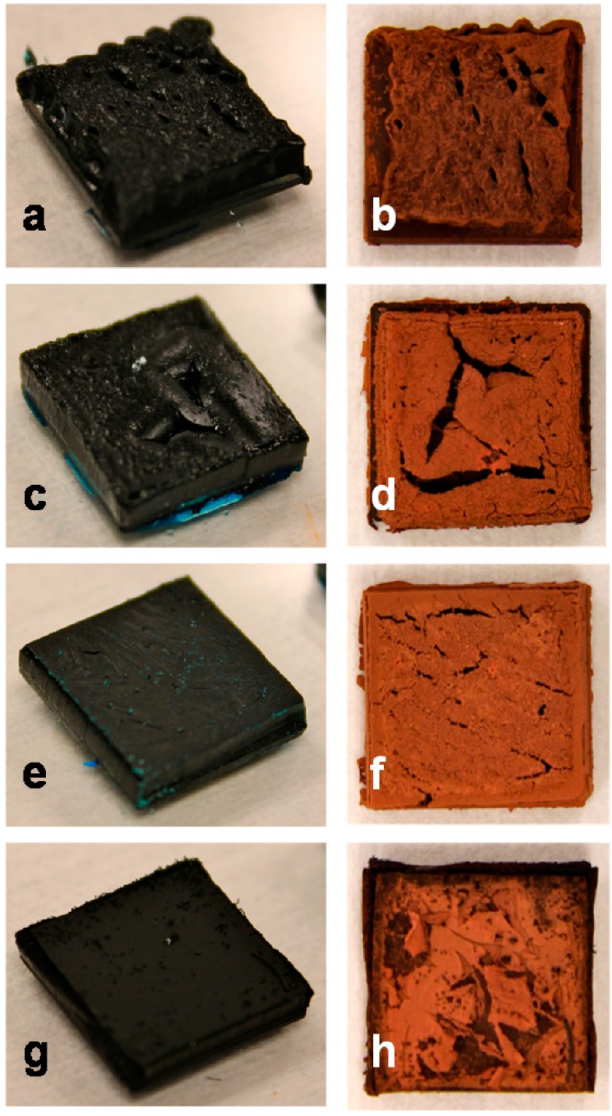

Figure 2. VACNT arrays exhibited differences in stability during composite fabrication on the basis of the duration of Py-C deposition. Py-C_0 after infiltration (a) and after reduction (b). Py-C_5 after infiltration (c) and after reduction (d). Py-C_30 after infiltration (e) and after reduction (f). Py-C_60 after infiltration (g) and after reduction (h). All sample dimensions are 13 mm (l) × 13 mm (w) × 2 mm.

many metals including Ni, Co, Fe, and Ag.[53] Using H_2 as the reducing agent is highly beneficial when compared to other routes. This is attributed to the relative ease of producing pure metals that require no further purification as well as the rapid reaction times because of better gas−solid interactions.

The microstructure of the Cu-VACNT composite made from Py-C_30 was characterized using SEM and is shown in Figure 4. The surfaces of individual MWCNTs are decorated in a dense network of Cu nanoparticles both throughout the cross-section (Figure 4a) and on the top surface of the array (Figure 4b). XRD analysis (Figure S3 in the Supporting Information) from the composite array confirmed total conversion of $Cu(NO_3)_2$ salt to CuO to metallic Cu after calcination and H_2 reduction, respectively.

Cu-VACNT composites were synthesized at both atmospheric (Cu-VACNT_Atm) and reduced pressure (Cu-VACNT_Vac) to compare the effect of pressure on Cu

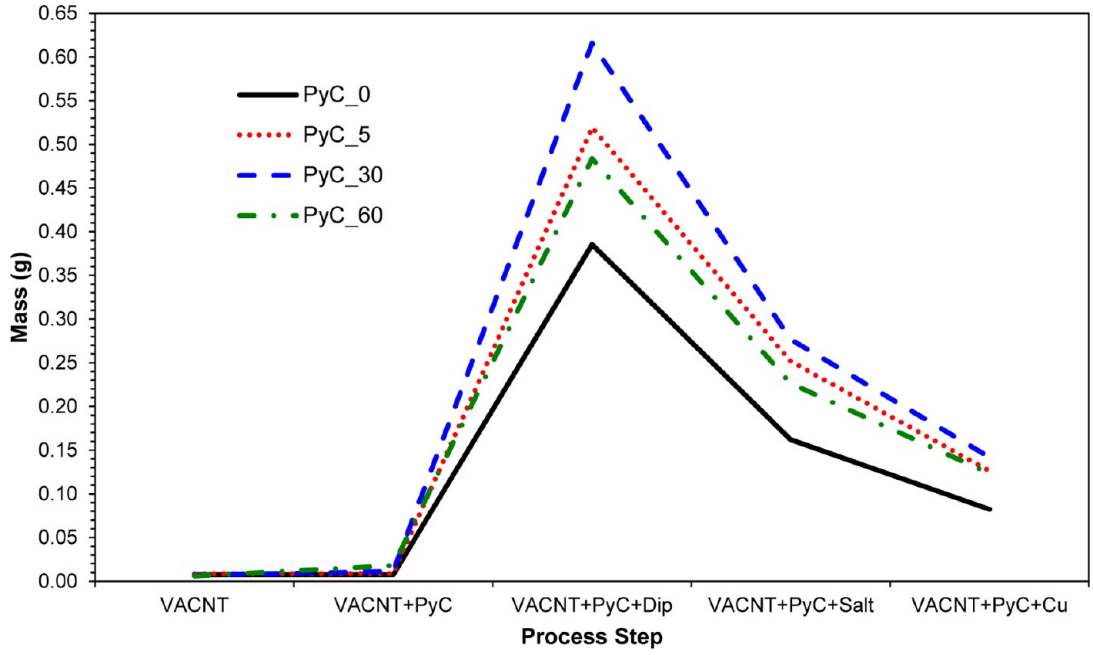

Figure 3. Duration of the Py-C deposition influenced the solution take-up upon infiltration as well as retention during drying and H_2 reduction. Py-C deposition for 30 min (Py-C_30) resulted in the highest concentration of Cu in the final composite.

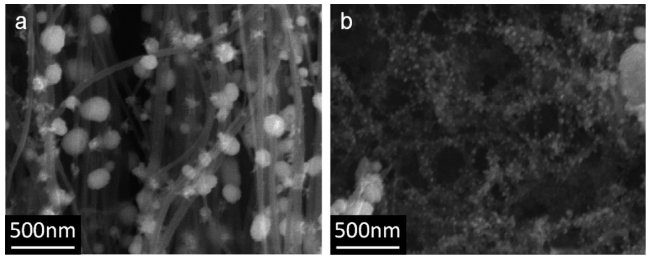

Figure 4. Microstructure of a Cu-VACNT composite made from copper(II) nitrate showing a dense network of Cu nanoparticles decorating MWCNT surfaces. (a) Scanning electron microscopy (SEM) micrograph of Cu-VACNT cross-section and (b) SEM micrograph of the top surface of Cu-VACNT.

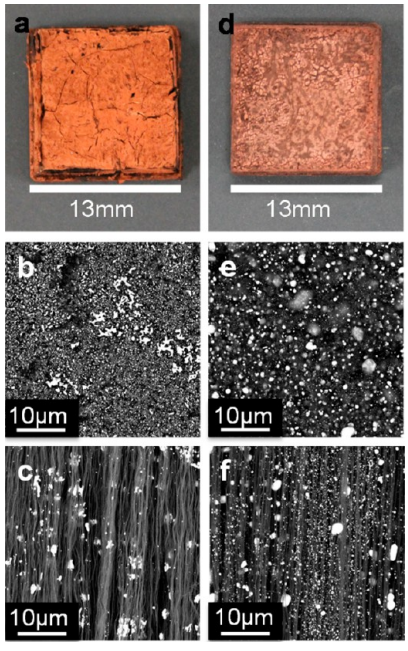

Figure 5. Cu-VACNT composites processed in vacuum (a–c) show a large gradient in Cu concentration between the (b) top and (c) cross-section of the sample. Cu-VACNT composites processed at atmospheric pressure (d–f) yielded a more even distribution of Cu throughout.

retention in the composites. For both samples, the theoretical Cu content (Cu_{th}) was calculated on the basis of the mass of $Cu(NO_3)_2$ salt measured in the sample after drying. Cu_{th} for both samples was compared to its respective measured Cu content (Cu_{act}). Cu_{act} of Cu-VACNT_Atm was 18% less than its Cu_{th}, whereas Cu_{act} for Cu-VACNT_Vac was 14%. $Cu(NO_3)_2$ is unstable at even slightly elevated temperature because of its high vapor pressure. The vapor pressures for $Cu(NO_3)_2$ during calcination at atmospheric pressure (225 °C) and under vacuum (185 °C) are around 3.59 and 0.99 Torr, respectively. This led to sublimation of the Cu salt during calcination regardless of the process pressure. This was confirmed by the presence of a very thin copper metal film on the inside of the process tube after the reduction step.

Although Cu-VACNT_Atm and Cu-VACNT_Vac retained similar percentages of Cu during processing, the distribution of Cu throughout the composite differed greatly. The Cu-VACNT_Vac sample developed a thick Cu coating on the top of the sample, which can be seen with the naked eye (Figure 5a). The SEM micrographs also showed a large difference in Cu concentration between the top of the composite (Figure 5b) and the cross-section (Figure 5c). Cu-VACNT_Atm, shown in Figure 5d–f, exhibited an even distribution of Cu throughout the entire sample.

To maximize Cu content in the VACNT arrays, an optimized procedure for multiple Cu salt solution infiltrations was developed. Three different samples were fabricated where the subsequent Cu salt infiltration was performed after one of three steps: drying (2Cu-VACNT_Dry), calcination (2Cu-VACNT_Cal), or reduction (2Cu-VACNT_Red). The total

weight increase from Cu added by both infiltrations was measured for each of the three samples.

Maximum Cu addition was measured for 2Cu-VACNT_Cal, with a total mass increase of 765%. Calcination removed bulky nitrate ions as well as water of hydration in the crystal. This process provided more free volume for $Cu(NO_3)_2$ solution to infiltrate during the second dip. Similarly, 2Cu-VACNT_Red increased in mass by over 650%. Reaction with H_2 gas reduced the CuO left after calcination to pure Cu. Because oxygen is more electronegative than pure copper, CuO is more likely than Cu to form hydrogen bonds with water molecules from the $Cu(NO_3)_2$ solution. 2Cu-VACNT_Dry had a much lower increase in mass, around 380%. The 12 h, 105 °C drying treatment immediately following infiltration removed only the water of solution from the VACNT array, leaving behind the bulky water of hydration and nitrate ions. This limited the amount of $Cu(NO_3)_2$ solution that infiltrated the array in subsequent dips.

Once the optimal processing pressure and method for incorporating a second infiltration were established, these parameters were implemented with the intent to maximize the number of infiltrations. As the SEM micrographs in Figure 6

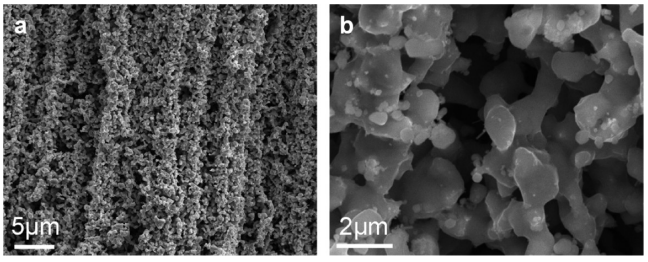

Figure 6. SEM micrographs of 5Cu_VACNT show that the vertically aligned MWCNT morphology is maintained in the array cross-section (a). SEM micrograph of the cross-section taken at higher magnification (b) shows the ends of individual MWCNTs that are visibly protruding from the Cu structure, indicating their total encapsulation.

illustrate, the VACNTs were not decorated but were rather encapsulated by the high volume of Cu after five infiltrations. Additionally, the vertical alignment of the MWCNTs was maintained throughout the array cross-section (Figure 6a). The individual and cumulative mass increases for five infiltrations are shown in Figure 7. After five infiltrations, the mass of the stabilized CNT array increased nearly 24-fold from the addition of Cu. Because of an abundance of free space within the CNT array, the initial mass increase following the first infiltration was quite large, around 680%. The second through fifth infiltrations resulted in decreased but consistent weight increases (between 30 and 60%), even after the fifth infiltration. This indicates that the VACNT array was not completely saturated and that additional infiltrations would continue to deposit Cu in the array.

XRD analysis (Figure 8) showed the CNTs' 002 reflection ~26° was visible after 1 infiltration, but because of the abundance of Cu in the array, the reflection was not visible after 2 infiltrations. Additionally, trace reflections from Cu_2O were measured for composites that were infiltrated 1 and 2 times. This was attributed to the formation of a native oxide layer on the Cu nanoparticle surface. In samples with up to 2 infiltrations, the added Cu retains a nanoparticle morphology. After 5 infiltrations, however, the Cu nanoparticles have

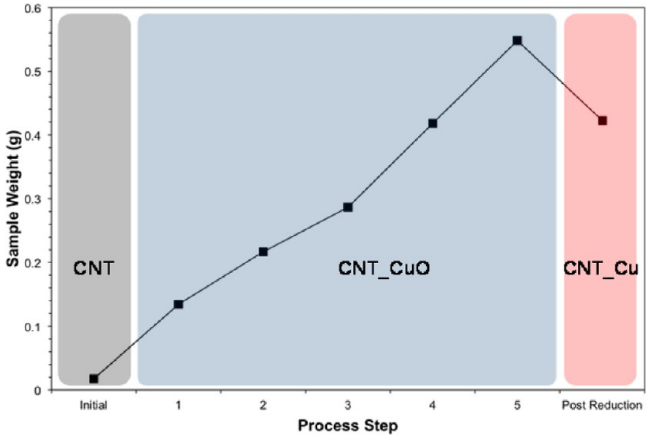

Figure 7. Cu content in VACNT arrays was maximized by infiltrating, drying, and calcinating the sample five times. The composite mass continuously increased with repeated infiltrations.

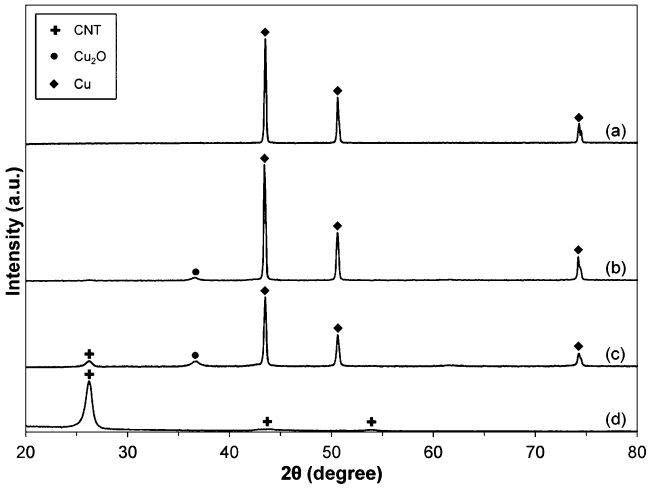

Figure 8. X-ray diffraction was used to monitor the change in CNT and Cu signal as a function of the number of infiltrations. After 5 infiltrations (a), only Cu reflections were visible. Following 1 and 2 infiltrations, however, (c and b, respectively), a reflection from Cu_2O ~36° was found because of the formation of native oxide on the high surface area Cu nanoparticles. Additionally, a small 002 reflection from CNTs ~26° was still visible on the 1 infiltration sample. Finally, a pristine VACNT array (d) was also analyzed as a control.

agglomerated, thus reducing their surface area to volume ratio of the copper.

Carbon nanotube-copper composites are attractive for thermal management applications and thermal interface materials because of their potentially high thermal conductivities.[11] According to energy carrier theory, the total thermal conductivity of a material is a sum of the contributions from both electron and phonon carriers. In metallically bonded materials like Cu (k = 385 W/mK), electrons are the dominant energy carrier. In individual MWNTs (k = 3000 W/mK[54]), ballistic transport of electrons and/or phonons along the tube axis gives rise to a dual conduction mechanism. Ideally, a composite comprising Cu and CNTs would exhibit a synergistic effect with both electrons and phonons as energy carriers and thus would exhibit greater thermal conductivity.

A problem arises when translating from individual CNTs to 3D assemblies. The bulk thermal conductivity of CNT arrays and buckypapers is low.[55] Heat transfer in CNTs is highly

anisotropic, with heat conductivity in the axial direction being 2 orders of magnitude larger than in the transverse direction.[56] The result is poor interfacial heat transfer created by the large thermal resistance between CNTs. This is due to weak intertube van der Waals bonding and limited tube−tube contact area. Additionally, because of their nanosized diameters and ultralow density when grown in an array, it is difficult to achieve ample contact area between CNTs and an electronic device. These characteristics create high contact resistance and the inability of the CNTs to spread heat laterally.[57] Finally, pristine VACNT arrays are extremely fragile and will irreparably deform with only slight disturbance.

The outlined method for preparing Cu-encapsulated VACNTs presents a solution to address all of these issues. Cu nanoparticles readily nucleate and densely cover the CNT surfaces. This is a result of O_2 plasma treatment that not only allowed the arrays to be wet by the Cu salt solutions but also provided functional groups with which Cu ions could interact and bond. Good interfacial bonding between CNTs and Cu promotes electron transfer and electron−phonon coupling.[58] Upon subsequent infiltrations, the particles grow and coalesce to form an interconnected network that coats the surface of individual CNTs and also bridges void space between adjacent CNTs. Binding adjacent CNTs with the Cu network may further promote electron transfer, improve heat spreading, increase contact area, and enhance mechanical rigidity. Not only do the CNTs remain unbundled but also the vertical alignment is preserved as a result of Py-C stabilization and infiltration with supersaturated Cu salt solutions. Furthermore, the procedure is scalable for even larger arrays and relies on rapid reactions at low processing temperatures.

4. CONCLUSIONS

Once the VACNT arrays were made wettable, it became apparent that measures needed to be taken to provide structural and dimensional stability to prevent array warping and cracking during composite fabrication. Py-C was shown to deposit conformally on individual CNTs, resulting in the radial growth of CNT diameters. This improved the CNT's resistance to buckling and also created a more dense and interconnected array structure. Although hybrid Cu-VACNT materials were successfully fabricated without CVD stabilization, deposition times of 30 and 60 min yielded stable arrays during composite fabrication. The former was able to take up more Cu salt solution, resulting in higher Cu content. SEM characterization of the composites exhibited Cu nanoparticles densely covering the CNT surfaces. Calcinating and reducing samples at atmospheric pressure provided an even distribution of Cu nanoparticles throughout the entire VACNT array cross-section when compared to those processed under vacuum.

The optimal stage for implementation of a second infiltration in the fabrication of Cu-VACNT composites with maximum Cu content is after calcination because of the large free volume created by the removal of water of solution, nitrate ions, and water of hydration as well as the compatibility of CuO with the aqueous salt solution. Multiple infiltrations were conducted through the process of reinfiltrating after drying and calcination. After five cycles and the final reduction, the mass of the VACNT array increased by 24-fold. Alignment of the MWCNTs was preserved throughout the process, and the MWCNTs appear to be completely encapsulated by Cu. This type of Cu-VACNT structure is highly sought after for thermal management structures. Future studies will assess the structural and thermal properties of these unique composites.

■ ASSOCIATED CONTENT

Supporting Information

EDS spectra taken during the conversion of $Cu(NO_3)_2$ to CuO and Cu. Photographs of Cu-CNT composites made from other copper salts. XRD analysis of the samples after each processing step. This material is available free of charge via the Internet at http://pubs.acs.org.

■ AUTHOR INFORMATION

Corresponding Author

*Fax: +1-919-515-6532; Tel: +1-919-515-1866; E-mail: philip_bradford@ncsu.edu.

Notes

The authors declare no competing financial interest.

■ ACKNOWLEDGMENTS

This material is based upon work supported by the National Science Foundation Graduate Research Fellowship Program under grant no. DGE-0946818. This work was also supported by the North Carolina Space Grant Consortium. We thank Prof. Yuntian Zhu for time on the Raman microscope, Chuck Mooney and Dale Batchelor for their assistance and expertise with microscopy, and Roberto Garcia for XRD characterization.

■ REFERENCES

(1) Planeix, J. M.; Coustel, N.; Coq, B.; Brotons, V.; Kumbhar, P. S.; Dutartre, R.; Geneste, P.; Bernier, P.; Ajayan, P. M. *J. Am. Chem. Soc.* **1994**, *116*, 7935−7936.
(2) Liu, Z.; Lin, X.; Lee, J. Y.; Zhang, W.; Han, M.; Gan, L. M. *Langmuir* **2002**, *18*, 4054−4060.
(3) Li, W.; Liang, C.; Zhou, W.; Qiu, J.; Sun, G.; Xin, Q. *J. Phys. Chem. B* **2003**, *107*, 6292−6299.
(4) Kong, J.; Chapline, M.; Dai, H. *Adv. Mater.* **2001**, *24*, 2000−2002.
(5) Sun, Y.; Wang, H. H. *Adv. Mater.* **2007**, *19*, 2818−2823.
(6) Fu, Y.; Zhang, L.; Chen, G. *Carbon* **2012**, *50*, 2563−2570.
(7) Kim, H.-S.; Lee, H.; Han, K.-S.; Kim, J.-H.; Song, M.-S.; Park, M.-S.; Lee, J.-Y.; Kang, J.-K. *J. Phys. Chem. B* **2005**, *109*, 8983−8986.
(8) Leela Mohana Reddy, A.; Ramaprabhu, S. *Int. J. Hydrogen Energy* **2007**, *32*, 3998−4004.
(9) Mohan, R.; Shanmugharaj, A. M.; Sung, R. H. *J. Biomed. Mater. Res., Part B* **2011**, *96*, 119−126.
(10) Ngo, Q.; Cruden, B. A.; Cassell, A. M.; Sims, G.; Meyyappan, M.; Li, J.; Yang, C. Y. *Nano Lett.* **2004**, *4*, 2403−2407.
(11) Chai, G.; Chen, Q. *J. Compos. Mater.* **2010**, *44*, 2863−2873.
(12) Chai, Y.; Zhang, K.; Zhang, M.; Chan, P. C. H.; Yuen, M. M. F. *Proc. − Electron. Components Technol. Conf.* **2007**, 1224−1229.
(13) Chu, K.; Wu, Q.; Jia, C.; Liang, X.; Nie, J.; Tian, W.; Gai, G.; Guo, H. *Compos. Sci. Technol.* **2010**, *70*, 298−304.
(14) Tu, J. P.; Yang, Y. Z.; Wang, L. Y.; Ma, X. C.; Zhang, X. B. *Tribol. Lett.* **2001**, *10*, 225−228.
(15) Chen, W. X.; Tu, J. P.; Wang, L. Y.; Gan, H. Y.; Xu, Z. D.; Zhang, X. B. *Carbon* **2003**, *41*, 215−222.
(16) Dong, S.; Tu, J.; Zhang, X. *Mater. Sci. Eng., A* **2001**, *313*, 83−87.
(17) Kim, K.; Cha, S. I.; Hong, S. *Mater. Sci. Eng., A* **2006**, *430*, 27−33.
(18) Li, H.; Misra, A.; Zhu, Y.; Horita, Z.; Koch, C. C.; Holesinger, T. G. *Mater. Sci. Eng., A* **2009**, *523*, 60−64.
(19) Ngo, Q.; Cruden, B. A.; Cassell, A. M.; Walker, M. D.; Ye, Q.; Koehne, J. E.; Meyyappan, M.; Li, J.; Yang, C. Y. *Mater. Res. Soc. Symp. Proc.* **2004**, *812*, 1−6.
(20) Male, K.; Hrapovic, S.; Liu, Y.; Wang, D.; Luong, J. *Anal. Chim. Acta* **2004**, *516*, 35−41.

(21) Ferrer-Anglada, N.; Gomis, V.; El-Hachemi, Z.; Weglikovska, U. D.; Kaempgen, M.; Roth, S. *Phys. Status Solidi* **2006**, *203*, 1082−1087.
(22) Arai, S.; Suwa, Y.; Endo, M. *J. Electrochem. Soc.* **2011**, *158*, D49−D53.
(23) Lin, Y.; Watson, K. A.; Fallbach, M. J.; Ghose, S.; Smith, J. G.; Delozier, D. M.; Cao, W.; Crooks, R. E.; Connell, J. W. *ACS Nano* **2009**, *3*, 871−84.
(24) Vennerberg, D.; Quirino, R.; Kessler, M. R. *Adv. Eng. Mater.* **2013**, *15*, 366−372.
(25) Cha, S. I.; Kim, K. T.; Arshad, S. N.; Mo, C. B.; Hong, S. H. *Adv. Mater.* **2005**, *17*, 1377−1381.
(26) Kim, K. T.; Cha, S. I.; Hong, S. H. *Mater. Sci. Eng., A* **2007**, *449−451*, 46−50.
(27) Kim, K. T.; Cha, S. I.; Gemming, T.; Eckert, J.; Hong, S. H. *Small* **2008**, *4*, 1936−1940.
(28) Chen, P.; Wu, X.; Lin, J.; Tan, K. L. *J. Phys. Chem. B* **1999**, *103*, 4559−4561.
(29) Chai, Y.; Sun, M.; Xiao, Z.; Li, Y.; Zhang, M. I. N.; Chan, P. C. H. *IEEE Nanotechnol.* **2011**, 11−13.
(30) Inoue, Y.; Kakihata, K.; Hirono, Y.; Horie, T.; Ishida, A.; Mimura, H. *Appl. Phys. Lett.* **2008**, *92*, 213113-1−213113-3.
(31) Gordon, S.; Campbell, C. *Anal. Chem.* **1955**, *27*, 1102−1109.
(32) Ghose, J.; Kanungo, A. *J. Therm. Anal.* **1981**, *20*, 459−462.
(33) Morozov, I. V.; Znamenkov, K. O.; Korenev, Y. M.; Shlyakhtin, O. A. *Thermochim. Acta* **2003**, *403*, 173−179.
(34) Wright, C. R. A.; Luff, A. P. *J. Chem. Soc.* **1878**, *33*, 1−27.
(35) Wright, C. R. A.; Luff, A. P.; Rennie, E. H. *J. Chem. Soc.* **1879**, *35*, 475−524.
(36) Pease, R. *J. Am. Chem. Soc.* **1921**, 820−826.
(37) Rodriguez, J. A.; Kim, J. Y.; Hanson, J. C.; Perez, M.; Frenkel, A. I. *Catal. Lett.* **2003**, *85*, 247−254.
(38) Bradford, P. D.; Wang, X.; Zhao, H.; Zhu, Y. T. *Carbon* **2011**, *49*, 2834−2841.
(39) Marmur, A. *Langmuir* **2003**, *19*, 8343−8348.
(40) Bico, J.; Thiele, U.; Quere, D. *Colloids Surf., A* **2002**, *206*, 41−46.
(41) Lau, K. K. S.; Bico, J.; Teo, K. B. K.; Chhowalla, M.; Amaratunga, G. A. J.; Milne, W. I.; McKinley, G. H.; Gleason, K. K. *Nano Lett.* **2003**, *3*, 1701−1705.
(42) Pierson, H. O. *Handbook of Carbon, Graphite, Diamond and Fullerenes: Properties, Processing and Applications*; Noyes Publishing: Park Ridge, NJ, 1993; pp 25−44.
(43) Pierson, H. O. *Handbook of Chemical Vapor Deposition*, 2nd ed.; Noyes Publishing: Norwich, NY, 1999; pp 161−169.
(44) Shafrin, E. G.; Zisman, W. A. *J. Phys. Chem.* **1960**, *64*, 519−524.
(45) Otten, A.; Herminghaus, S. *Langmuir* **2004**, *20*, 2405−2408.
(46) *Surface Modification of Nanotube Fillers*; Mittal, V., Ed.; Wiley-VCH Verlag GmbH & Co.: Weinheim, Germany, 2011.
(47) Souza Filho, A. G.; Jorio, A.; Samsonidze, G. G.; Dresselhaus, G.; Saito, R.; Dresselhaus, M. S. *Nanotechnology* **2003**, *14*, 1130−1139.
(48) Thomsen, C.; Reich, S. *Phys. Rev. Lett.* **2000**, *85*, 5214−5217.
(49) Vix-Guterl, C.; Couzi, M.; Dentzer, J.; Trinquecoste, M.; Delhaes, P. *J. Phys. Chem. B* **2004**, *108*, 19361−19367.
(50) Hurst, K. E.; Dillon, A. C.; Yang, S.; Lehman, J. H. *J. Phys. Chem. C* **2008**, *112*, 16296−16300.
(51) Mattia, D.; Gogotsi, Y. *Microfluid. Nanofluid.* **2008**, *5*, 289−305.
(52) Ramos, S. C.; Vasconcelos, G.; Antunes, E. F.; Lobo, A. O.; Trava-Airoldi, V. J.; Corat, E. J. *Diamond Relat. Mater.* **2010**, *19*, 752−755.
(53) Luidold, S.; Antrekowitsch, H. *JOM* **2007**, *59*, 58−62.
(54) Kim, P.; Shi, L.; Majumdar, A.; McEuen, P. *Phys. Rev. Lett.* **2001**, *87*, 19−22.
(55) Gonnet, P.; Liang, Z.; Choi, E.; Kadambala, R.; Zhang, C.; Brooks, J. S.; Wang, B.; Kramer, L. *Curr. Appl. Phys.* **2006**, *6*, 119−122.
(56) Che, J.; Cagin, T.; Goddard, W. A. *Nanotechnology* **2000**, *11*, 65−69.
(57) Prasher, R. *Nano Lett.* **2005**, *5*, 2155−2159.
(58) Xu, Z.; Buehler, M. J. *ACS Nano* **2009**, *3*, 2767−2775.